Augmented moment method for stochastic ensembles with delayed couplings. II. FitzHugh-Nagumo model

Hideo Hasegawa*
Department of Physics, Tokyo Gakugei University, Koganei, Tokyo 184-8501, Japan
(Received 18 November 2003; revised manuscript received 2 April 2004; published 27 August 2004)

Dynamics of FitzHugh-Nagumo (FN) neuron ensembles with time-delayed couplings subject to white noises, has been studied by using both direct simulations and a semianalytical augmented moment method (AMM) which has been proposed in a preceding paper [H. Hasegawa, Phys. Rev. E **70**, 021911 (2004)]. For N-unit FN neuron ensembles, AMM transforms original $2N$-dimensional *stochastic* delay differential equations (SDDEs) to infinite-dimensional *deterministic* DEs for means and correlation functions of local and global variables. Infinite-order recursive DEs are terminated at the finite level m in the level-m AMM (AMMm), yielding $8(m+1)$-dimensional deterministic DEs. When a single spike is applied, the oscillation may be induced if parameters of coupling strength, delay, noise intensity and/or ensemble size are appropriate. Effects of these parameters on the emergence of the oscillation and on the synchronization in FN neuron ensembles have been studied. The synchronization shows the *fluctuation-induced* enhancement at the transition between nonoscillating and oscillating states. Results calculated by AMM5 are in fairly good agreement with those obtained by direct simulations.

DOI: 10.1103/PhysRevE.70.021912 PACS number(s): 87.10.+e, 84.35.+i, 05.45.−a, 07.05.Mh

I. INTRODUCTION

There have been many studies on effects of noises in dynamical systems with delays. Complex behavior due to noise and delay is found in many systems such as biological systems, signal transmissions, electrical circuits, and lasers. Systems with both noises and delay are commonly described by stochastic delay differential equations (SDDEs). In recent years, linear and nonlinear SDDEs of Langevin equation are beginning to gain much attention [1–7]. The parameter range for the stationary solutions of the Langevin equation has been examined with the use of the step by step method [1], the moment mothod [2], and the Fokker-Planck equation (FPE) method [3,4].

When we turn our attention to living brains, various kinds of noises are reported to be ubiquitous. A study on noise effects has been one of major recent topics in neuronal systems. It has been shown that the response of neurons may be improved by background noises. The typical example is the stochastic resonance in which weak noises enhance the transmission of signals with the subthreshold level. The transmission delay is inherent because the speed of spikes propagating through axons is finite. Conduction velocity ranges from 20 to 60 m/s, leading to non-negligible transmission times from milliseconds to hundreds milliseconds. Although an importance of effects of delay has been not so recognized as that of noises, there is an increasing interest in the complex behavior of time delays, whose effects have been investigated by using integrate-and-fire (IF) [8–12], FitzHugh-Nagumo (FN) [13–15], Hindmarsh-Rose (HR) [16], and Hodgkin-Huxley (HH) models [10,11,17,18]. Exposed behaviors due to time delays are the multistability and bifurcation leading to chaos.

There are two difficulties in studying combined effects of noise and delay in brains. One is that the system is usually described by *nonlinear* SDDEs, which are generally more difficult than linear SDDEs. Dynamics of individual neurons includes a variety of voltage dependent ionic channels which can be described by nonlinear DEs of Hodgkin-Huxley-type models, or of reduced neuron models such as IF, FN, and HR models. The other difficulty is that a small cluster of cortex consists of thousands of similar neurons. For a study of dynamics of noisy neuron ensembles with time-delayed couplings, we have to solve high-dimensional nonlinear SDDEs, which have been studied by direct simulations (DSs) [19,20] and by analytical methods like FPE [21]. Simulations for large-scale neuron ensembles have been made mostly by using IF, FN, HR and phase models. Since the time to simulate networks by conventional methods grows as N^2 with N, the size of the ensemble, it is rather difficult to simulate realistic neuron clusters. Although FPE is a powerful method in dealing with the stochastic DE, a simple FPE application to SDDE fails because of its non-Markovian property [3,5].

In a preceding paper [22] (which is referred to hereafter as I), the present author has developed an augmented moment method (AMM) for SDDE, employing a semianalytical dynamical mean-field approximation (DMA) theory [23,24]. In I, AMM is applied to an ensemble described by the delay Langevin model, transforming the original N-dimensional SDDEs to infinite-dimensional DEs which are terminated at finite level m in the level-m AMM (AMMm). Model calculations in I with changing the level m have shown that calculated results converge at a fairly small m. Actually results obtained by AMM6 are in good agreement with those by DSs for linear and nonlinear Langevin ensembles. It has been demonstrated in I that AMM may be a useful tool in discussing dynamics and synchronization of ensembles described by SDDEs.

It is the purpose of the present paper to apply AMM to FN neuron ensembles with time-delayed couplings. In Sec. II,

*Email address: hasegawa@u-gakugei.ac.jp

we apply our AMM theory to nonlinear SDDEs of N-unit FN neuron ensembles, in order to get the infinite-dimensional deterministic DEs for the correlation functions of local and global variables. Infinite-dimensional recursive DEs are terminated at the finite level m in AMMm. In Sec. III we report model calculations, showing that results of our AMM are in good agreement with those of DSs. Section IV is devoted to conclusions and discussions.

II. FN NEURON ENSEMBLE

A. Adopted model and method

Dynamics of a neuron ensemble consisting of N-unit FN neurons ($N \geqslant 2$), is described by the $2N$-dimensional nonlinear SDDEs given by

$$\frac{dx_{1i}(t)}{dt} = F[x_{1i}(t)] - cx_{2i}(t) + \left(\frac{1}{N-1}\right)\sum_{j(\neq i)} w_{ij}G(x_{1j}(t-\tau_{ij})) + \xi_i(t) + I^{(e)}(t), \tag{1}$$

$$\frac{dx_{2i}(t)}{dt} = bx_{1i}(t) - dx_{2i}(t) + e \quad (i = 1-N), \tag{2}$$

where $F[x(t)]=kx(t)[x(t)-h][1-x(t)]$, $k=0.5$, $h=0.1$, $b=0.015$, $c=1.0$, $d=0.003$, and $e=0$ [23,25], and x_{1i} and x_{2i} denote the fast (voltage) and slow (recovery) variables, respectively. The third term in Eq. (1) stands for interactions with the uniform couplings of $w_{ij}=w$ and delay times of $\tau_{ij}=\tau$, and the sigmond function $G(x)$ given by $G(x)=1/(1+\exp[-(x-\theta)/\alpha])$, θ and α denoting the threshold and the width, respectively [26]. The all-to-all couplings have been widely employed in theoretical studies. The assumed constant delay may be justified in certain neural networks [27]. The fourth term of Eq. (1), $\xi_i(t)$, denotes the Gaussian white noise given by $\langle \xi_i(t)\rangle = 0$ and $\langle \xi_i(t)\xi_j(t')\rangle = \beta^2\delta_{ij}\delta(t-t')$ where β denotes the magnitudes of independent noises and the bracket $\langle\cdot\rangle$ the stochastic average [28]. The last term in Eq. (1), $I^{(e)}(t)$, denotes an external input whose explicit form will be shown later [Eq. (31)].

We apply our AMM developed in I to FN neuron ensemble given by Eqs. (1) and (2), defining global variables for the ensemble given by

$$X_\kappa(t) = \frac{1}{N}\sum_i x_{\kappa i}(t), \quad \kappa = 1,2, \tag{3}$$

and their averages by

$$\mu_\kappa(t) = \langle X_\kappa(t)\rangle. \tag{4}$$

We define the correlation functions between local variables, given by

$$\gamma_{\kappa,\lambda}(t,t') = \frac{1}{N}\sum_i \langle \delta x_{\kappa i}(t)\delta x_{\lambda i}(t')\rangle, \quad \kappa,\lambda = 1,2, \tag{5}$$

where $\delta x_{\kappa i}(t) = x_{\kappa i}(t) - \mu_\kappa(t)$. Similarly we define the correlation function between global variables, given by

$$\rho_{\kappa,\lambda}(t,t') = \langle \delta X_\kappa(t)\delta X_\lambda(t')\rangle \tag{6}$$

$$= \frac{1}{N^2}\sum_i\sum_j \langle \delta x_{\kappa j}(t)\delta x_{\lambda i}(t')\rangle, \tag{7}$$

where $\delta X_\kappa(t) = X_\kappa(t) - \mu_\kappa(t)$. Conventional variances and covariances are given by Eqs. (5)–(7) with $t=t'$, for which the symmetry relations: $\gamma_{1,2}(t,t) = \gamma_{2,1}(t,t)$ and $\rho_{1,2}(t,t) = \rho_{2,1}(t,t)$, are held. It is noted that $\gamma_{\kappa,\nu}(t,t)(\kappa,\lambda = 1,2)$ expresses the spatial average of fluctuations in local variables of $x_{\kappa i}$ while $\rho_{\kappa,\nu}(t,t)$ denotes fluctuations in global variables of X_κ.

After our previous studies [22–24], we have assumed that the noise intensity β is weak and that the distribution of state variables takes the Gaussian form concentrated near the means of (μ_1,μ_2). The second assumption is justified from numerical calculations for single FN [29,30] and HH neurons [31,32]. We will obtain infinite-order equations of motions for means, variance, and covariances defined by Eqs. (5)–(7). They will be terminated at the level m in AMM m. Readers who are not interested in mathematical details, may skip to Sec. II C.

B. Equations of motions

After some manipulations, we get DEs for $\mu_\kappa(t)$, $\gamma_{\kappa,\nu}(t,t)$ and $\rho_{\kappa,\nu}(t,t)(\kappa,\nu = 1,2)$ given by (for details see Appendix A)

$$\frac{d\mu_1(t)}{dt} = f_0(t) + f_2(t)\gamma_{1,1}(t,t) - c\mu_2(t) + w\, u_0(t-\tau) + I^{(e)}(t), \tag{8}$$

$$\frac{d\mu_2(t)}{dt} = b\mu_1(t) - d\mu_2(t) + e, \tag{9}$$

$$\frac{d\gamma_{1,1}(t,t)}{dt} = 2[a(t)\gamma_{1,1}(t,t) - c\gamma_{1,2}(t,t)] + 2wu_1(t-\tau)\zeta_{1,1}(t,t-\tau) + \beta^2, \tag{10}$$

$$\frac{d\gamma_{2,2}(t,t)}{dt} = 2[b\gamma_{1,2}(t,t) - d\gamma_{2,2}(t,t)], \tag{11}$$

$$\frac{d\gamma_{1,2}(t,t)}{dt} = b\gamma_{1,1}(t,t) + [a(t)-d]\gamma_{1,2}(t,t) - c\gamma_{2,2}(t,t) + wu_1(t-\tau)\zeta_{2,1}(t,t-\tau), \tag{12}$$

$$\frac{d\rho_{1,1}(t,t)}{dt} = 2[a(t)\rho_{1,1}(t,t) - c\rho_{1,2}(t,t)] + 2wu_1(t-\tau)\rho_{1,1}(t,t-\tau) + \frac{\beta^2}{N}, \tag{13}$$

$$\frac{d\rho_{2,2}(t,t)}{dt} = 2[b\rho_{1,2}(t,t) - d\rho_{2,2}(t,t)], \tag{14}$$

$$\frac{d\rho_{1,2}(t,t)}{dt} = b\rho_{1,1}(t,t) + [a(t) - d]\rho_{1,2}(t,t) - c\rho_{2,2}(t,t) + wu_1(t-\tau)\rho_{2,1}(t,t-\tau), \quad (15)$$

with

$$a(t) = f_1(t) + 3f_3(t)\gamma_{1,1}(t,t), \quad (16)$$

$$u_0(t) = g_0(t) + g_2(t)\gamma_{1,1}(t,t), \quad (17)$$

$$u_1(t) = g_1(t) + 3g_3(t)\gamma_{1,1}(t,t), \quad (18)$$

$$\zeta_{\kappa,\nu}(t,t') = \left(\frac{1}{N-1}\right)[N\rho_{\kappa,\nu}(t,t') - \gamma_{\kappa,\nu}(t,t')], \quad (19)$$

where $f_\ell(t) = (1/\ell!)F^{(\ell)}(\mu_1(t))$ and $g_\ell(t) = (1/\ell!)G^{(\ell)}(\mu_1(t))$. Equations (8)–(15) include the higher-order terms of $\gamma_{\kappa,\nu}(t,t-\tau)$ and $\rho_{\kappa,\nu}(t,t-\tau)$, whose equations of motions are given by $(m \geqslant 1)$

$$\frac{d\gamma_{1,1}(t,t-m\tau)}{dt} = [a(t) + a(t-m\tau)]\gamma_{1,1}(t,t-m\tau) - c[\gamma_{1,2}(t,t-m\tau) + \gamma_{2,1}(t,t-m\tau)] + w[u_1(t-\tau)\zeta_{1,1}(t-\tau,t-m\tau) + u_1(t-(m+1)\tau)\zeta_{1,1}(t,t-(m+1)\tau)] + \beta^2\Delta(m\tau), \quad (20)$$

$$\frac{d\gamma_{2,2}(t,t-m\tau)}{dt} = b[\gamma_{1,2}(t,t-m\tau) + \gamma_{2,1}(t,t-m\tau)] - 2d\gamma_{2,2}(t,t-m\tau), \quad (21)$$

$$\frac{d\gamma_{1,2}(t,t-m\tau)}{dt} = b\gamma_{1,1}(t,t-m\tau) + [a(t) - d]\gamma_{1,2}(t,t-m\tau) - c\gamma_{2,2}(t,t-m\tau) + wu_1(t-\tau) \times \zeta_{1,2}(t-\tau,t-m\tau), \quad (22)$$

$$\frac{d\gamma_{2,1}(t,t-m\tau)}{dt} = b\gamma_{1,1}(t,t-m\tau) + [a(t-m\tau) - d] \times \gamma_{2,1}(t,t-m\tau) - c\gamma_{2,2}(t,t-m\tau) + wu_1(t-(m+1)\tau)\zeta_{2,1}(t,t-(m+1)\tau), \quad (23)$$

$$\frac{d\rho_{1,1}(t,t-m\tau)}{dt} = [a(t) + a(t-m\tau)]\rho_{1,1}(t,t-m\tau) - c[\rho_{1,2}(t,t-m\tau) + \rho_{2,1}(t,t-m\tau)] + w[u_1(t-\tau)\rho_{1,1}(t-\tau,t-m\tau) + u_1(t-(m+1)\tau)\rho_{1,1}(t,t-(m+1)\tau)] + \left(\frac{\beta^2}{N}\right)\Delta(m\tau), \quad (24)$$

$$\frac{d\rho_{2,2}(t,t-m\tau)}{dt} = b[\rho_{1,2}(t,t-m\tau) + \rho_{2,1}(t,t-m\tau)] - 2d\rho_{2,2}(t,t-m\tau), \quad (25)$$

$$\frac{d\rho_{1,2}(t,t-m\tau)}{dt} = b\rho_{1,1}(t,t-m\tau) + [a(t) - d]\rho_{1,2}(t,t-m\tau) - c\rho_{2,2}(t,t-m\tau) + wu_1(t-\tau) \times \rho_{1,2}(t-\tau,t-m\tau), \quad (26)$$

$$\frac{d\rho_{2,1}(t,t-m\tau)}{dt} = b\rho_{1,1}(t,t-m\tau) + [a(t-m\tau) - d] \times \rho_{2,1}(t,t-m\tau) - c\rho_{2,2}(t,t-m\tau) + wu_1(t-(m+1)\tau)\rho_{2,1}(t,t-(m+1)\tau), \quad (27)$$

where $\Delta(x) = 1$ for $x = 0$ and 0 otherwise.

C. Summary of our method

The original two-dimensional SDDE given by Eqs. (1) and (2) are transformed to infinite-dimensional deterministic DDEs given by Eqs. (8)–(15) and (20)–(27), which are due to non-Markovian property of SDDE. It is, however, impossible to simultaneously solve these infinite-order recursive equations. We will adopt the level-m AMM (AMMm) in which the recursive DEs are terminated at the finite level m, as

$$\gamma_{\kappa,\nu}(t,t-(m+1)\tau) = \gamma_{\kappa,\nu}(t,t-m\tau), \quad (28)$$

$$\rho_{\kappa,\nu}(t,t-(m+1)\tau) = \rho_{\kappa,\nu}(t,t-m\tau), \quad (29)$$

$$g_1(t-(m+1)\tau) = g_1(t-m\tau), \quad (30)$$

leading to $8(m+1)$-dimensional DEs. In the following Sec. III, we will examine AMMm, performing calculations with changing m, in order to show that AMM5 may yield results in fairy good agreement with those of DS [Fig. 5(b)]. In the limit of $\tau = 0$, Eqs. (20)-(27) reduce to Eqs. (10)–(15), then Eqs. (8)–(15) agree with Eqs. (20)–(27) in Ref. [23] for FN neurons ensembles without delays [26].

Model calculations will be reported in the following Sec. III. DSs have been performed for $2N$ DEs given by Eqs. (1) and (2) by using the fourth-order Runge-Kutta method with a time step of 0.01. Initial values of variables at $t \in (-\tau, 0]$ are $x_i(t) = y_i(t) = 0$ for $i = 1$ to N. DS results are the average of 100 trials otherwise noticed. AMM calculations have been performed for Eqs. (8)–(30) by using also the fourth-order Runge-Kutta method with a time step of 0.01. Initial values are $\mu_1(t) = \mu_2(t) = 0$ at $t \in [-\tau, 0]$, and $\gamma_{\kappa,\nu}(t,t') = \rho_{\kappa,\nu}(t,t') = 0$ $t \in [-\tau, 0]$ or $t' \in [-\tau, 0] (t \geqslant t')$. All calculated quantities are dimensionless.

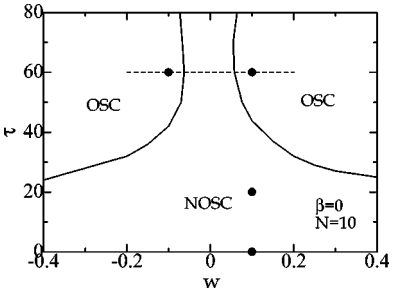

FIG. 1. The $w-\tau$ phase diagram showing the oscillating (OSC) and nonoscillating (NOSC) states for $\beta=0$ and $N=10$. For sets of parameters of w and τ marked by circles, time courses of $\mu(t)$, $\gamma(t,t)$, $\rho(t,t)$, and $S(t)$ are calculated, whose results are shown in Figs. 2 and 3. Along the horizontal dashed line ($\tau=60$), the w dependence of σ_o and σ_s is calculated in Figs. 4 and 5.

III. MODEL CALCULATIONS

A. Effects of coupling (w) and delay (τ)

In this study, we pay our attention to the response of the FN neuron ensembles to a single spike input of $I^{(e)}(t)$ given by [23]

$$I^{(e)}(t) = A\ \Theta(t - t_{\rm in})\Theta(t_{\rm in} + T_w - t), \tag{31}$$

where $\Theta(x)=1$ for $x>0$ and 0 otherwise, A stands for the magnitude, $t_{\rm in}$ the input time and T_w the spike width. We have adopted the same parameters of $A=0.10$, $t_{\rm in}=100$, and $T_w=10$ as in Ref. [23]. Parameter values of w, τ, β, and N will be explained shortly.

When an input spike given by Eq. (31) is applied, the oscillation may be triggered when model parameters are appropriate. The $w-\tau$ phase diagram showing the oscillating (OSC) and nonoscillating (NOSC) states is depicted in Fig. 1, which is calculated for $\beta=0$ and $N=10$. In the case of $\beta=0.01$, for example, the OSC region is slightly shrunk compared to that for $\beta=0$, as will be shortly discussed [Figs. 5(a) and 5(b)]. The $w-\tau$ phase is separated by two boundaries in positive- and negative-w regions. Circles in Fig. 1 express pairs of w and τ adopted for calculations to be shown in Figs. 2 and 3. Along the horizontal, dashed line in Fig. 1, the w value is continuously changed in calculations to be shown in Figs. 4(a) and 4(b).

In order to monitor the emergence of the oscillation, we calculate the quantity:

$$\sigma_o = \overline{O(t)} = \frac{1}{t_2 - t_1}\int_{t_1}^{t_2} dt\ O(t), \tag{32}$$

with

$$O(t) = \frac{1}{N}\sum_i \left[\langle x_i(t)^2\rangle - \langle x_i(t)\rangle^2\right] \tag{33}$$

$$= \mu(t)^2 - \mu(t)^2 + \gamma_{1,1}(t), \tag{34}$$

which becomes finite in the oscillation state but vanishes in the nonoscillating state, the overline denoting the temporal average between $t_1(=2000)$ and $t_2(=4000)$.

The synchrony within ensembles is measured by [22,23]

$$\sigma_s = \overline{S(t)}, \tag{35}$$

with

$$S(t) = \left(\frac{N\rho_{1,1}(t,t)/\gamma_{1,1}(t,t) - 1}{N-1}\right), \tag{36}$$

which is 0 and 1 for completely asynchronous and synchronous states, respectively.

We have calculated time courses of $\mu_1(t)$, $\gamma_{1,1}(t,t)$, $\rho_{1,1}(t,t)$, and $S(t)$, whose results are depicted in Figs. 2(a)–2(l), solid and dashed curves denoting results of AMM and DS, respectively.

For $\tau=0$, an output spike of $\mu_1(t)$ fires after an applied input which is plotted at the bottom of Fig. 2(a) [and also of Figs. 2(e) and 2(i)]. It is noted that state variables are randomized when an input spike is applied at $t=100$ because independent noises have been added since $t=0$. Figures 2(b) and 2(c) show $\gamma_{1,1}$ and $\rho_{1,1}$ for $\tau=0$, respectively. The synchronization ratio $S(t)$ for $\tau=0$ shown in Fig. 2(d) has an appreciable magnitude: its maximum values calculated in AMM are 0.038 and 0.077 at $t=107$ and 123, respectively. Figure 2(e) shows that when a delay of $\tau=20$ is introduced, an input signal leads to a spike output with an additional, small peak in μ_1 at $t=133$. Figures 2(f) and 2(g) show that although a peak of $\gamma_{1,1}$ for $\tau=20$ becomes larger than that for $\tau=0$, a peak of $\rho_{1,1}$ is decreased by an introduced delay. Maximum values of $S(t)$ calculated by AMM are 0.154 and 0.130 at $t=126$ and 140, respectively, for $\tau=20$. We note from Fig. 2(i) that for a larger $\tau=60$, an input spike triggers an autonomous oscillation with a period of about 65. Peaks in $\gamma_{1,1}$, $\rho_{1,1}$, and S are progressively increased with increasing t as shown in Figs. 2(j)–2(l): peaks of $\gamma_{1,1}$, $\rho_{1,1}$, and S saturate at $t\gtrsim 1200$ with the values of 0.00253, 0.00014, and 0.098, respectively, in AMM calculations. We note in Figs. 2(a)–2(l) that results of μ_1 obtained by AMM and DS are indistinguishable, and that AMM results of $\gamma_{1,1}$, $\rho_{1,1}$, and S are in fairly good agreement with those of DSs.

Figure 1 shows that although the obtained NOSC-OSC phase is nearly symmetric with respect to the $w=0$ axis, it is not in the strict sense. Actually the property of the oscillation for inhibitory couplings ($w<0$) is different from that for excitatory couplings ($w>0$). Figures 3(a) and 3(b) show autonomous oscillations for $w=0.1$ and $w=-0.1$, respectively, with $\tau=60$, $\beta=0.01$, and $N=10$. The period of the oscillation T is given by $T=\tau+\tau_i$ where τ_i denotes the intrinsic delay for firings. For inhibitory feedback with negative w, FN neurons fire with the rebound process, which requires a larger τ_i for firing than for excitatory feedback with positive w. Then the period of $T=86$ for autonomous oscillation with the negative w becomes larger than that of $T=65$ with the positive w.

By changing the w value along the horizontal, dashed line in Fig. 1, we have calculated the w dependence of σ_o and σ_s, whose results are plotted in Figs. 4(a) and 4(b), respectively, for $\beta=0.0001$ and 0.01. The oscillation emerges for $w\gtrsim 0.058$ or $w\lesssim -0.063$ with $\beta=0.0001$, while with $\beta=0.01$ it occurs for $w\gtrsim 0.060$ or $w\lesssim -0.070$. The transition from NOSC to OSC states is of the first order because σ_o is abruptly increased at the critical coupling of $w=w_c$, where σ_s

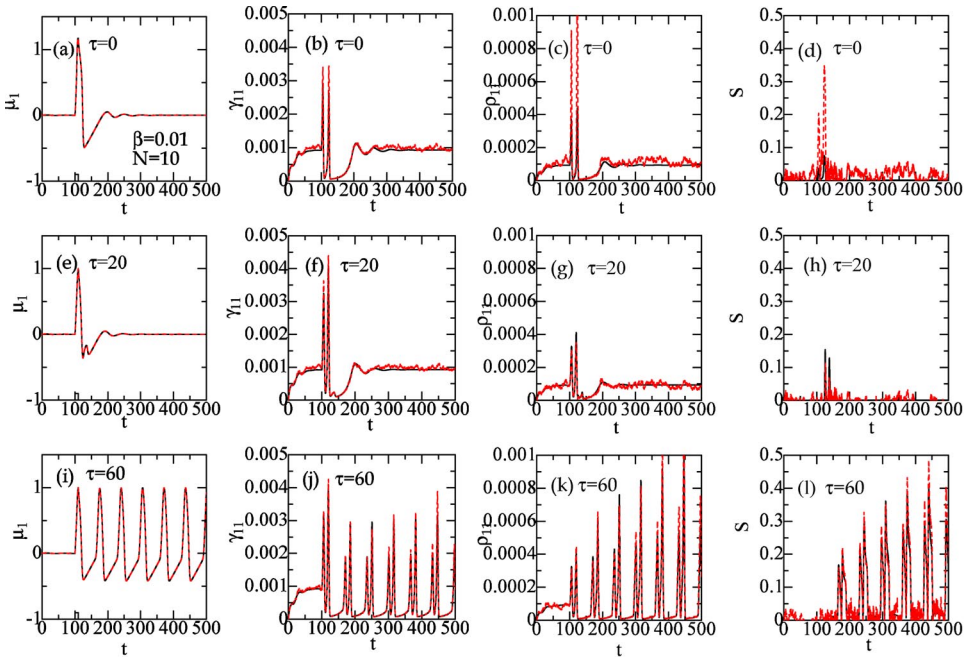

FIG. 2. (Color online) Time courses of $\mu_1(t)$, $\gamma_{1,1}(t)$, $\rho_{1,1}(t)$, and $S(t)$ calculated by AMM theory (solid curves) and DS (dashed curves) with $A=0.10$, $\beta=0.01$, $w=0.1$, and $N=10$: (a) μ_1, (b) $\gamma_{1,1}$, (c) $\rho_{1,1}$, and (d) S for $\tau=0$, (e) μ_1, (f) $\gamma_{1,1}$, (g) $\rho_{1,1}$, and (h) S for $\tau=20$, and (i) μ_1, (j) $\gamma_{1,1}$, (k) $\rho_{1,1}$, and (ℓ) S for $\tau=60$. Chain curves at bottoms of (a), (e), and (i) express input spikes.

has a narrow peak. In contrast, the relevant NOSC-OSC transition in the nonlinear Langevin model is of the second order [22].

We have investigated, in more detail, the w dependence of σ_o and σ_s near the transition region of $0.05 \leqslant w \leqslant 0.07$, which is sandwiched by vertical, dashed lines in Figs. 4(a) and 4(b), results for $\beta=0.0001$ and $\beta=0.01$ being plotted in Figs. 5(a) and 5(b), respectively. Figure 5(a) shows that the critical w value for the NOSC-OSC transition is $w_c \simeq 0.0579$ for $\beta=0.0001$ both in DS and AMM5. When we adopt AMM1, we get the result showing the NOSC-OSC transition at $w \sim 0.6$, although we cannot get solutions for $0.0586 < w < 0.060$. With the use of AMM2, we get the transition at $w \sim 0.058$, though solutions are not obtainable for $0.0580 < w < 0.0582$. We have noted that AMM m converges at the level $m=3$, above which calculated results are almost identical. Figure 5(b) shows that the critical value of w_c for $\beta=0.01$ is 0.0600 in DS and 0.0607 in AMM5. For $m=1$, 2, and 3, the NOSC-OSC transition occurs at $w=$ 0.0644, 0.0609, and 0.0807, respectively: w_c for $m=3$ approaches that for $m=5$ (in what follows results of AMM5 will be reported). It is interesting to note in Figs. 5(a) and 5(b) that the synchrony σ_s shows *fluctuation-induced* enhancement at the NOSC-OSC transition. This is due to an increase in the ratio of $\rho_{1,1}(t,t)/\gamma_{1,1}(t,t)$ in Eq. (36) although both $\rho_{1,1}(t,t)$ and $\gamma_{1,1}(t,t)$ are increased at the NOSC-OSC transition. Similar phenomenon has been reported in the nonlinear Langevin model [22] and in heterogeneous systems in which the oscillation emerges when the degree of the heterogeneity exceeds the critical value [33,34].

B. Effects of noise (β)

Comparing Fig. 5(b) with Fig. 5(a), we note that when the noise intensity is increased form $\beta=0.0001$ to $\beta=0.01$, the critical w_c value for the NOSC-OSC transition is increased: $w_c=0.0579$ (0.0579) for $\beta=0.001$ and $w_c=0.0600$ (0.0607) for $\beta=0.01$ in DS (AMM). Figure 6(a) shows the β dependence of σ_o and σ_s for $\tau=60$, $w=0.06$ and $N=10$. σ_o is rapidly decreased at $\beta \sim \beta_c$ where σ_s has a broad peak: β_c is about 0.01 in DS while it is about 0.0075 in AMM. Figure 6(b) shows that the similar β dependence of σ_o and σ_s is obtained also for a larger $w=0.062$, for which $\beta_c \sim 0.015$ in DS and $\beta_c \sim 0.014$ in AMM. A suppression of the oscillation by noises is realized in the Langevin model [22] and in some calculations for systems with heterogeneity [34], although the noise-induced oscillation is reported in Refs. [21,35,36]. In particular, Zorzano and Vázquez [21] (ZV) showed the noise-induced oscillation in FN neuron ensembles ($N=\infty$) with time delays by using FPE method. The difference between ZV's results and ours may be due to the difference in the adopted FN model and/or ensemble size. In order to get some insight on this issue, we have performed AMM calculations for our FN model with larger ensemble sizes of $N=100$ and 1000, and obtained again a suppression of the oscillation by noises [37]. It is not clear for us how ZV took into account the non-Markovian property of SDDE within their FPE method [3,5].

C. Effects of size (N)

The N dependence of σ_o and σ_s for $\beta=0.01$, $w=0.06$ and $\tau=60$ is shown in Fig. 7 where open circles (squares) express $\sigma_o(\sigma_s)$ in DS, and where thin (bold) solid curves denote $\sigma_o(\sigma_s)$ in AMM. It is shown that with increasing the size of ensemble, σ_o is gradually increased at $N \sim N_c$ where σ_s has a broad peak, the critical dimension being $N_c \sim 10$ in DS and $N_c \sim 100$ in AMM. Results of our AMM calculations are

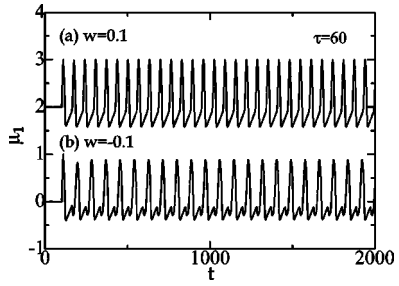

FIG. 3. Time courses of $\mu_1(t)$ showing the oscillation for (a) $w=0.1$ and (b) $w=-0.1$ with $\tau=60$, $\beta=0.01$, and $N=10$ calculated by AMM, the result of (a) being shifted upwards by 2.

qualitatively similar to those of DS although calculated N_c values are different between the two methods.

IV. CONCLUSIONS AND DISCUSSIONS

In Sec. II, we have obtained the infinite-dimensional ordinary differential equations. It is, however, possible to get expressions given by partial differential equations (PDEs) if we define the correlation functions:

$$C_{\kappa,\lambda}(t,z) = \frac{1}{N}\sum_i \langle \delta x_{\kappa i}(t)\, \delta x_{\lambda i}(t-z)\rangle, \tag{37}$$

$$D_{\kappa,\lambda}(t,z) = \langle \delta X_\kappa(t)\, \delta X_\lambda(t-z)\rangle, \tag{38}$$

introducing a new variable z [see Eqs. (5) and (6)]. For example, PDEs for $C_{1,1}(t,z)$ are given by

$$\frac{\partial C_{1,1}(t,0)}{\partial t} = 2[aC_{1,1}(t,0) - cC_{1,2}(t,0)] + 2wu_1(t-\tau)E_{1,1}(t,\tau) + \beta^2, \tag{39}$$

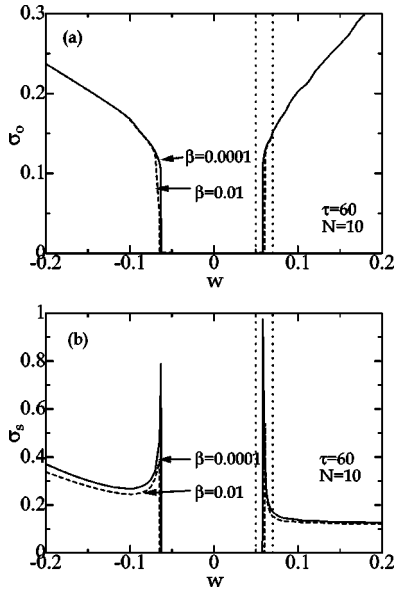

FIG. 4. The w dependence of (a) σ_o and (b) σ_s for $\beta=0.0001$ (solid curves) and $\beta=0.01$ (dashed curves) with $\tau=60$ and $N=10$. The region sandwiched by dashed, vertical lines is enlarged in Figs. 5(a) and 5(b) for $\beta=0.0001$ and 0.01, respectively.

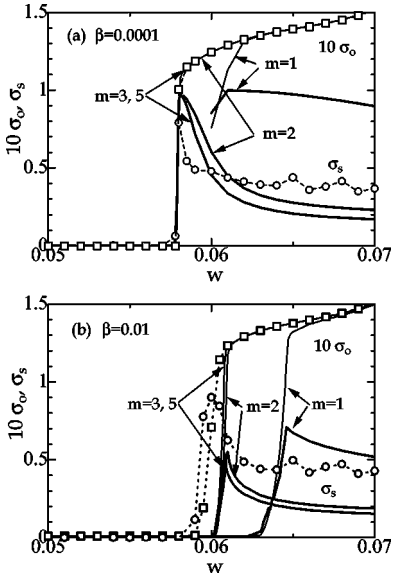

FIG. 5. The w dependence of σ_o and σ_s for (a) $\beta=0.0001$ and (b) $\beta=0.01$ with $\tau=60$ and $N=10$. Thin and bold solid curves denote results of $10\sigma_o$ and σ_s, respectively, in AMM, whereas squares and circles express those of $10\sigma_o$ and σ_s, respectively, in DS. AMM results with different level $m(=1,2,3,\text{and } 5)$ are shown. Dotted lines are only for a guide of the eye (see text).

$$\left(\frac{\partial}{\partial t} + \frac{\partial}{\partial z}\right) C_{1,1}(t,z) = aC_{1,1}(t,z) - cC_{1,2}(t,z) + wu_1(t-\tau)E_{1,1}(t-\tau,z-\tau) \quad \text{for} \quad z>0, \tag{40}$$

where $E_{1,1}(t,z)=[ND_{1,1}(t,z)-C_{1,1}(t,z)]/[N-1]$. It is noted

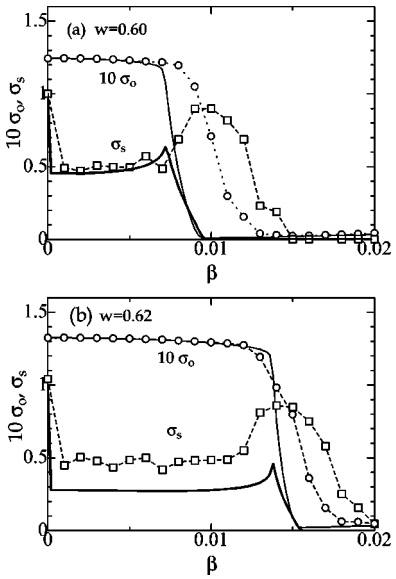

FIG. 6. The β dependence of σ_o and σ_s for (a) $w=0.60$ and (b) $w=0.62$ with $\tau=60$ and $N=10$. Thin and bold solid curves denote results of $10\sigma_o$ and σ_s, respectively, in AMM whereas squares and circles express those of $10\sigma_o$ and σ_s, respectively, in DS. Dotted lines are only for a guide of the eye.

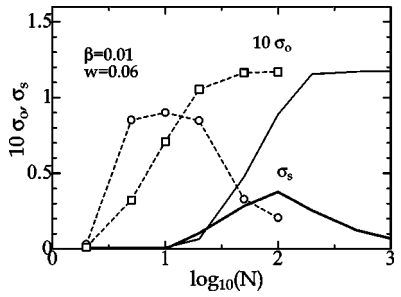

FIG. 7. The N dependence of σ_o and σ_s for $\beta=0.01$, $\tau=60$, and $w=0.06$. Thin and bold solid curves denote results of $10\sigma_o$ and σ_s, respectively, in AMM, whereas squares and circles express those of $10\sigma_o$ and σ_s, respectively, in DS. Dotted lines are only for a guide of the eye.

that Eqs. (39) and (40) correspond to Eqs. (10) and (20), respectively. Then we have to solve PDEs including $\mu_\kappa(t)$, $C_{\kappa,\lambda}(t,z)$, and $D_{\kappa,\lambda}(t,z)$ with a proper boundary condition in the (t,z) space. A similar PDE approach has been adopted in Ref. [6] for an analysis of the stationary solution of the linear Langevin equation with delays. In an earlier stage of this study, we pursued the PDE approach. We realized, however, from the point of computer programming that the use of the ordinary DEs given in AMM is more tractable than that of PDEs.

Our calculations have shown that FN neuron ensembles with delays exhibit the multistability when model parameters such as w, τ, β, and N are varied. The multistability is the common property of the system with time delay. Actually the nonlinear Langevin ensembles discussed in I also show the multistability: the $w-\tau$ phase diagram of FN ensembles shown in Fig. 1 is similar to that of the Langevin ensembles shown in Fig. 6 of I. In either case, *fluctuation-induced* synchronization is realized near the transition between OSC and NOSC states. These results imply that the oscillating, highly synchronous state may be realized in ensembles for smaller couplings with a proper delay than with no delays. This is consistent with the recent result of Ref. [38], where the importance of delays is stressed for the long-range synchronization with low coupling strength.

In summary, we have discussed dynamics of FN neuron ensembles with delays by using a semi-analytical method developed in I. Our method has a limitation of weak noises but it is free from the magnitude of delay times. This is complementary to the small-delay approximation [3], whose application to FN neuron ensembles with delays is discussed in Appendix C. For FN ensembles to show the oscillation, we have to adopt an appreciable magnitude of delay ($\tau \gtrsim 20$), for which SDA method cannot be employed. In this study we have discussed only the case of a single spike input. Our method may be, however, applicable to arbitrary inputs such as periodic spike trains and Poisson spikes, as was made for HH neuron ensembles (without delays) [24]. Although results calculated by our method are in fairly good agreement with those obtained by DC, the quantitative analytical theory is still lacking. In this study, we have assumed regular couplings ($w_{ij}=w$) and uniform time delays ($\tau_{ij}=\tau$). In real systems, however, couplings are neither regular nor random, and time delays are nonuniform with a variety of dendrite radius and length. It is interesting to include these properties by extending our approach, which is in progress and will be reported in a future paper [39].

ACKNOWLEDGMENT

This work is partly supported by a Grant-in-Aid for Scientific Research from the Japanese Ministry of Education, Culture, Sports, Science, and Technology.

APPENDIX A: DERIVATION OF EQS. (8)–(15)

We express Eqs. (1) and (2) in a Taylor expansion of $\delta x_i(=\delta x_{1i})$ and $\delta y_i(=\delta x_{2i})$ up to the third-order terms to get

$$\frac{d\delta x_i(t)}{dt} = f_1(t)\,\delta x_i(t) + f_2[\delta x_i(t)^2 - \gamma_{1,1}(t,t)] + f_3(t)\,\delta x_i(t)^3 - c\,\delta y_i(t) + \xi_i(t) + \delta I_i^{(c)}(t-\tau), \tag{A1}$$

$$\frac{d\delta y_i(t)}{dt} = b\,\delta x_i(t) - d\,\delta y_i(t), \tag{A2}$$

with

$$\delta I_i^{(c)}(t) = w\left(\frac{g_1(t)}{N-1}\sum_{j(\neq i)}\delta x_j(t) + \frac{g_2(t)}{N-1}\sum_{j(\neq i)}[\delta x_j(t)^2 - \gamma_{1,1}] + \frac{g_3(t)}{N-1}\sum_{j(\neq i)}\delta x_j(t)^3\right), \tag{A3}$$

where $f_\ell(t)=(1/\ell!)F^{(\ell)}(\mu_1(t))$ and $g_\ell(t)=(1/\ell!)G^{(\ell)}(\mu_1(t))$. Averages of Eqs. (A1) and (A2) with Eqs. (3) and (4) yield DEs for means of $d\mu_1/dt$ and $d\mu_2/dt$ [Eq. (8)]. DEs for variances and covariances may be obtained by using the equations of motions of δx_i and δy_i. For example, DE for $d\gamma_{1,2}(t,t)/dt$ is given by

$$\frac{d\gamma_{1,2}(t,t)}{dt} = \frac{1}{N}\sum_i\left\langle\left(\frac{d\delta x_i(t)}{dt}\right)\delta y_i(t) + \delta x_i(t)\left(\frac{d\delta y_i(t)}{dt}\right)\right\rangle, \tag{A4}$$

which leads to Eq. (12). DEs for other variances and covariances are similarly obtained.

APPENDIX B: DERIVATION OF EQS. (20)–(27)

In the process of calculations of Eqs. (8)–(15), we get new correlation functions given by

$$S_1(t_1,t_2) = \frac{1}{N}\sum_i\langle\delta x_i(t_1)\xi_i(t_2)\rangle, \tag{B1}$$

$$S_2(t_1,t_2) = \frac{1}{N}\sum_i\langle\delta y_i(t_1)\xi_i(t_2)\rangle, \tag{B2}$$

where $\delta x_i=\delta x_{1i}$, $\delta y_i=\delta x_{2i}$, $t_1=t$ and $t_2=t-m\tau$, or $t_1=t-m\tau$ and $t_2=t$. We will evaluate them by using DEs for $\delta x_i(t)$ and $\delta y_i(t)$, which are linearized from Eqs. (A1)–(A3):

$$\frac{d\delta x_i(t)}{dt} = a(t)\delta x_i(t) - c\delta y_i(t) + \left(\frac{w}{N-1}\right)\sum_{j(\neq i)} g_1(t-\tau)\delta x_j(t-\tau) + \xi_i(t), \tag{B3}$$

$$\frac{d\delta y_i(t)}{dt} = b\delta x_i(t) - d\delta y_i(t), \tag{B4}$$

where $a(t)=f_1(t)+3f_3(t)\gamma_{1,1}(t,t)$. Neglecting the t dependence in $a(t)$, we get formal solutions of Eqs. (B3) and (B4) given by

$$\delta x_i(t) = \left(\frac{A+d}{A-B}\right)\int^t ds\ \exp^{(t-s)A} \times\left[\left(\frac{w}{N-1}\right)\sum_{j(\neq i)} g_1(s-\tau)\delta x_j(s-\tau) + \xi_i(s)\right] - \left(\frac{B+d}{A-B}\right)\int^t ds\ \exp^{(t-s)B} \times\left[\left(\frac{w}{N-1}\right)\sum_{j(\neq i)} g_1(s-\tau)\delta x_j(s-\tau) + \xi_i(s)\right], \tag{B5}$$

$$\delta y_i(t) = \left(\frac{b}{A-B}\right)\int^t ds\ \exp^{(t-s)A} \times\left[\left(\frac{w}{N-1}\right)\sum_{j(\neq i)} g_1(s-\tau)\delta x_j(s-\tau) + \xi_i(s)\right] - \left(\frac{b}{A-B}\right)\int^t ds\ \exp^{(t-s)B} \times\left[\left(\frac{w}{N-1}\right)\sum_{j(\neq i)} g_1(s-\tau)\delta x_j(s-\tau) + \xi_i(s)\right], \tag{B6}$$

where A and B are roots of the equation given by $z^2-(a-d)z-ad+bc=0$. By using the method of steps in Ref. [6], we obtain the step by step functions, from which we get

$$S_1(t,t-m\tau) = S_1(t-m\tau,t) = \left(\frac{\beta^2}{2}\right)\Delta(m\tau), \tag{B7}$$

$$S_2(t,t-m\tau) = S_2(t-m\tau,t) = 0, \tag{B8}$$

where $\Delta(x)=1$ for $x=0$ and 0 otherwise. By using Eqs. (B7) and (B8), we get Eqs. (20)–(27). The assumption of a neglect of the t dependence in $a(t)$ may be justified, to some extent, from results calculated by our method which are in fairly good agreement with those by DS as reported in Sec. III.

APPENDIX C: THE SMALL-DELAY APPROXIMATION

When the delay τ is very small, we may adopt the small-delay approximation (SDA) proposed in Ref. [3]. With this approximation, we first transform the SDDEs to stochastic non-delayed DEs, and then to deterministic DEs with the use of DMA [23]. For a small τ, we may expand $x_{1i}(t-\tau)$ in Eq. (1) as

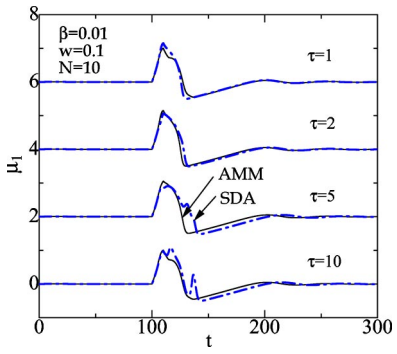

FIG. 8. The time course of $\mu_1(t)$ calculated in AMM (solid curves) and in a small-delay approximation (SDA) (chain curves) with $\beta=0.01$, $w=0.1$, and $N=10$, results for $\tau=5,2$, and 1 being successively shifted upwards by 2 (see Appendix C).

$$x_{1i}(t-\tau) \simeq x_{1i}(t) - \tau\frac{dx_{1i}(t)}{dt}, \tag{C1}$$

with which Eq. (1) becomes stochastic nondelayed DEs given by

$$\frac{dx_{1i}(t)}{dt} + \left(\frac{w\tau}{N-1}\right)\sum_{j(\neq i)} G'(x_{1j}(t))\frac{dx_{1j}(t)}{dt} = F(x_{1i}) - cx_{i2} + \left(\frac{w}{N-1}\right)\sum_{j(\neq i)} G(x_{1j}(t)(+\xi_i(t) + I^{(e)}. \tag{C2}$$

When we apply DMA to $2N$-dimensional stochastic DEs given by Eqs. (2) and (C2), we get equations of motions for means, variances and covariances, given by

$$\frac{d\mu_1(t)}{dt} = [1-w\tau u_1][f_0(t) + f_2(t)\gamma_{1,1}(t,t) - c\mu_2(t) + wg_0(t) + I^{(e)}(t)], \tag{C3}$$

$$\frac{d\mu_2(t)}{dt} = b\mu_1(t) - d\mu_2(t) + e, \tag{C4}$$

$$\frac{d\gamma_{1,1}(t,t)}{dt} = 2[a(t)\gamma_{1,1}(t,t) - c\gamma_{1,2}(t,t) + wu_1(t)\zeta_{1,1}(t,t)] + \beta^2 - 2w\tau u_1(t)\left[a(t)\zeta_{1,1}(t,t) - c\zeta_{1,2}(t,t) + \left(\frac{wu_1(t)}{N-1}\right) \times(N\rho_{1,1}(t,t) - \zeta_{1,1}(t,t))\right], \tag{C5}$$

$$\frac{d\gamma_{2,2}(t,t)}{dt} = 2[b\gamma_{1,2}(t,t) - d\gamma_{2,2}(t,t)], \tag{C6}$$

$$\frac{d\gamma_{1,2}(t,t)}{dt} = b\gamma_{1,1}(t,t) + [a(t)-d]\gamma_{1,2}(t,t) - c\gamma_{2,2}(t,t) + wu_1(t)\zeta_{1,2}(t,t) - w\tau u_1(t)\left[a(t)\zeta_{1,2}(t,t) - c\zeta_{2,2}(t,t) + \left(\frac{wu_1(t)}{N-1}\right)(N\rho_{1,2}(t,t) - \zeta_{1,2}(t,t))\right], \tag{C7}$$

$$\frac{d\rho_{1,1}(t,t)}{dt} = 2[1-w\tau u_1(t)]\left[a(t)\rho_{1,1}(t,t) - c\rho_{1,2}(t,t) + wu_1(t)\rho_{1,1}(t,t) + \frac{\beta^2}{2N}\right], \tag{C8}$$

$$\frac{d\rho_{2,2}(t,t)}{dt} = 2[b\rho_{1,2}(t,t) - d\rho_{2,2}(t,t)], \tag{C9}$$

$$\frac{d\rho_{1,2}(t,t)}{dt} = b\rho_{1,1}(t,t) + [a(t)-d]\rho_{1,2}(t,t) - c\rho_{2,2}(t,t) + wu_1(t)\rho_{1,2}(t,t) - w\tau u_1(t)[a(t)\rho_{1,2}(t,t) - c\rho_{2,2}(t,t) + wu_1(t)\rho_{1,2}(t,t)], \tag{C10}$$

where $a(t)$ and $\zeta_{\kappa,\lambda}(t,t)$ are given by Eqs. (16) and (19), respectively.

A numerical comparison between AMM and SDA is made in Fig. 8, where solid and chain curves denote results of AMM and SDA, respectively. For $\tau=0$ both methods lead to the identical result. For small delays of $\tau=1$ and 2, results of SDA are in fairly good agreement with those of AMM. As the delay is increased to $\tau>5$, however, the discrepancy between the two methods becomes significant.

[1] U. Küchler and B. Mensch, Stoch. Stoch. Rep. **40**, 23 (1992).
[2] M. C. Mackey and I. G. Nechaeva, Phys. Rev. E **52**, 3366 (1995).
[3] S. Guillouzic, I. L'Heureux, and A. Longtin, Phys. Rev. E **59**, 3970 (1999).
[4] T. Ohira and T. Yamane, Phys. Rev. E **61**, 1247 (2000).
[5] T. D. Frank and P. J. Beek, Phys. Rev. E **64**, 021917 (2001).
[6] T. D. Frank, P. J. Beek, and R. Friedrich, Phys. Rev. E **68**, 021912 (2003).
[7] D. Huber, and L. S. Tsimring, Phys. Rev. Lett. **91**, 260601 (2003).
[8] C. M. Marcus and R. M. Westervelt, Phys. Rev. A **39**, 347 (1989).
[9] C. van Vreeswijk, L. F. Abbott, and G. B. Ermentrout, J. Comput. Neurosci. **1**, 303 (1994).
[10] J. Foss, A. Longtin, B. Mensour, and J. Milton, Phys. Rev. Lett. **76**, 708 (1996).
[11] K. Pakdaman, J. Vibert, E. Bousssard, and N. Azmy, Neural Networks **9**, 797 (1996).
[12] U. Ernst, K. Pawelzik, and T. Geisel, Phys. Rev. E **57**, 2150 (1998).
[13] R. E. Plant, SIAM (Soc. Ind. Appl. Math.) J. Appl. Math. **40**, 150 (1981).
[14] S. R. Campbell and D. Wang, Physica D **111**, 151 (1998).
[15] S. A. Campbell and M. Waite, Nonlin. Anal. **47**, 1093 (2001).
[16] M. G. Rosenblum and A. S. Pikovsky, Phys. Rev. Lett. **92**, 114102 (2004).
[17] M. Park and S. Kim, J. Korean Phys. Soc. **29**, 9 (1996).
[18] H. Hasegawa, J. Phys. Soc. Jpn. **69**, 3726 (2000).
[19] S. Kim, S. H. Park, and C. S. Ryu, Phys. Rev. Lett. **79**, 2911 (1997).
[20] R. Borisyuk, BioSystems **67**, 3 (2002).
[21] M. P. Zorzano and L. Vázquez, Physica D **179**, 105 (2003).
[22] H. Hasegawa, Phys. Rev. E **70**, 021911 (2004).
[23] H. Hasegawa, Phys. Rev. E **67**, 041903 (2003).
[24] H. Hasegawa, Phys. Rev. E **68**, 041909 (2003).
[25] R. Rodriguez and H. C. Tuckwell, Phys. Rev. E **54**, 5585 (1996).
[26] The normalization factor of the coupling term is $(N-1)^{-1}$ in this paper while it is N^{-1} in Ref. [21]; results of the latter are obtainable from those of the former by a replacement of $\omega \rightarrow \omega(N-1/N)$.
[27] M. Salami, C. Itami, T. Tsumoto, and F. Kimura, Proc. Natl. Acad. Sci. U.S.A. **100**, 6174 (2003).
[28] The bracket of $\langle G(\mathbf{z},t)\rangle$ denotes the average (or the expectation value) of an arbitrary function $G(\mathbf{z},t)$ of N FN neuron ensembles, defined by $\langle G(\mathbf{z},t)\rangle = \int\cdots\int d\mathbf{z}\, G(\mathbf{z},t)p(\mathbf{z})$, where $p(\mathbf{z})$ denotes a probability distribution function (pdf) for $2N$-dimensional random variables of $\mathbf{z} = (x_1,\ldots,x_N,y_1,\ldots,y_N)^t$.
[29] H. C. Tuckwell and R. Rodriguez, J. Comput. Neurosci. **5**, 91 (1998).
[30] S. Tanabe and K. Pakdaman, Phys. Rev. E **63**, 031 911 (2001).
[31] S. Tanabe, S. Sato, and K. Pakdaman, Phys. Rev. E **60**, 7235 (1999).
[32] S. Tanabe and K. Pakdaman, Biol. Cybern. **85**, 269 (2001).
[33] J. H. E. Cartwright, Phys. Rev. E **62**, 1149 (2000).
[34] C. D. E. Boschi, E. Louis, and G. Ortega, Phys. Rev. E **65**, 012901 (2001).
[35] B. Hu and C. Zhou, Phys. Rev. E **61**, R1001 (2000).
[36] G. De Vries and A. Sherman, Bull. Math. Biol. **63**, 371 (2001).
[37] Although we tried to perform AMM calculations by using the same FN model as Zorzano and Vázquez (ZV) adopted (Ref. [21]), we could not do it because the form of the network coupling of ZV was rather different from ours.
[38] M. Dhamala, V. K. Jirsa, and M. Ding, Phys. Rev. Lett. **92**, 074 104 (2004).
[39] H. Hasegawa, e-print cond-mat/0403415.